Eur. Phys. J. D **29**, 63–68 (2004)
DOI: 10.1140/epjd/e2004-00006-6

THE EUROPEAN PHYSICAL JOURNAL D

Electrostatic model calculations of fission barriers for fullerene ions

H. Zettergren[a], J. Jensen, H.T. Schmidt, and H. Cederquist

Physics Department, Stockholm University, AlbaNova University Center, 10691 Stockholm, Sweden

Received 5 November 2003 / Received in final form 10 December 2003
Published online 27 January 2004 – © EDP Sciences, Società Italiana di Fisica, Springer-Verlag 2004

Abstract. We present model calculations of kinetic energy releases and fission barriers in asymmetric fission of C_{60}^{r+} ions, using a simple electrostatic model where the fragments are treated as conducting spheres. The kinetic energy releases are calculated using two different approaches for deducing the radii of the spheres. Both approaches give results in qualitative agreement with experimental results. The fission barriers, on the other hand, depend strongly on the model radii and the activation energies for neutral fragment emission. A comparison between the model calculations shows that the choice of the finite size of the smaller fragments become important as r increases and have large influences on the prediction for the C_{60}^{r+} stability limit. The competition between neutral (evaporation) and charged-fragment emission (fission) are discussed within a static over-the-barrier model for electron transfer between conducting spheres.

PACS. 34.70.+e Charge transfer – 36.40.Qv Stability and fragmentation of clusters – 36.40.Wa Charged clusters

1 Introduction

The fragmentation of multiply charged finite systems has attracted theoretical as well as experimental attention during the last century (see [1] and references therein). The Liquid Drop Model (LDM) has successfully been used to model properties of microscopic droplets [2], nuclei [3,4] and clusters [5–8]. In the LDM, the spherical form of a classical charged droplet is shown to be stable for displacement when the coulomb energy (E_c) is less than twice the cohesive surface energy (E_s), i.e. when the fissility parameter defined as $\chi = E_c/2E_s$ is smaller than 1. The competition between the cohesive surface energy and the repulsive coulomb energy yields a barrier, which cease to exist when $\chi = 1$ (the Rayleigh limit). The height of the barrier has to be compared with the activation energy for emission of neutral particles in order to determine whether the droplet will decay predominantly via fission or evaporation. In order to take shell effects in metal clusters into account, a shell correction method (developed for nuclear fission [9]) has proven to be useful to reproduce experimental results in more detail [10]. High level calculations such as molecular-dynamic (MD) simulations used for small cluster sizes [11,12] and jellium calculations for larger clusters [13], have so far not been used to determine fission barriers for highly charged *fullerene* ions.

In this work we use a simple electrostatic model to calculate the kinetic energy releases and fission barriers for the processes

$$C_{60}^{r+} \rightarrow C_{60-2m}^{(r-1)+} + C_{2m}^{+} \quad (1)$$

where $m = 1{-}2$ and $r = 1{-}16$. The purpose is to investigate the limitations and validity of this model. To our knowledge, model calculations of fission barriers for highly charged fullerenes have only been performed in conjunction with experimental studies of branching ratios for different fission channels [14] and the stability limit of charged C_{60}^{r+} [15]. In these cases, the fission barrier height was deduced from the interaction energy between the fission partners and the difference in total binding energy of the final and initial states, $\Delta E = E_f - E_i$ (which is given by the binding energies per atom and the ionization energies of the fission partners). A common problem is to determine the latter parameters for high charge states using a consistent theoretical method. High level calculations of e.g. ionization energies for C_{60}^{r+} have been performed [16–18], but only for r up to 12 [18].

Highly charged ions, used as projectiles in collision studies, have proven to be efficient tools for removing electrons from fullerenes creating stable or metastable fullerene ions. Experimental results using Xe^{8+}- [19] and Xe^{30+}-ions [20] showed that evaporation is favoured for low charge states r ($r < 4$), asymmetric fission dominates for intermediate r, and multifragmentation becomes competitive for $r = 6$. Asymmetric fission was however observed up to $r = 9$ [20,21], showing that C_{60}^{r+} ions are produced at low internal energies. The highest charge state observed under ion impact (Xe^{25+}-projectiles) is C_{60}^{10+} [22]

[a] e-mail: henning@physto.se

while C_{60}^{12+} was observed using infrared femtosecond laser fields [23].

The Auto-Charge-Transfer (ACT) process, i.e. the emission of a neutral light fragment from the parent ion followed by an electron transfer from the neutral to the charged fragment, was proposed in 1995 as an interpretation of measured kinetic energy releases in the asymmetric fission of C_{60}^{r+} ($r = 3-7$) [24,25]. Recently, however, Tomita et al. [26] and Cederquist et al. [15] showed that their measured kinetic energy releases in the fission of C_{60}^{r+} ($r = 4-8$ and $r = 6-9$, respectively) can be explained without the ACT process. Instead the concept of a reaction barrier was adopted, which we will give additional support for in this work.

The remainder of this work is organized as follows. In Section 2 we deduce an expression for the fission barrier of a metal cluster, using a simple electrostatic model [27] for the interaction between two conducting spheres. Here, electron transfer during the process is considered, whereas the description of the sphere-sphere interaction is identical to the one by Näher et al. [28]. In Section 3 we compare experimental and model kinetic energy releases in the asymmetric fission processes, $C_{60}^{r+} \rightarrow C_{60-2m}^{(r-1)+} + C_{2m}^{+}$ ($2m = 2, 4$). We then deduce fission barriers for $2m = 2-4$ as functions of the initial C_{60} charge and discuss the competition between the different fragmentation processes. We will also discuss the ACT process [24]. According to the present model, this process is only possible if the classical over-the-barrier criterion is fulfilled. That is when the Stark-shifted ionization potential is smaller than the maximum of the potential which an electron experiences as it moves between the fragments [27]. In the following sections, we will use atomic units unless otherwise stated.

2 Model

We model the fragmentation of an arbitrary charged metal cluster (A) under the assumption that the two separating fragments (B and C) are conducting spheres. The mutual polarization of the two spheres is described by two infinite series of image charges (one in each sphere) as described by Zettergren et al. [27] and Näher et al. [28]. The sphere-sphere interaction energy is

$$U_{int}(R) = \frac{1}{2}\left[\frac{q^B\left[q_0^B(R) - q^B\right]}{a^B} + \frac{q^C\left[q_0^C(R) - q^C\right]}{a^C}\right], \quad (2)$$

where q^B and q^C are the net fragment charges, $q_0^B(R)$ and $q_0^C(R)$ are the center charges, and a^B and a^C are the sphere radii. The magnitudes of the center charges are given by the infinite series of image charges [27,28], which in turn depend on the sphere radii, net charges, and the center-center distance R. For $R = \infty$, $q_0^B = q^B$ and $q_0^C = q^C$, yielding zero interaction energy ($U_{int} = 0$). When one sphere radius is set to zero (e.g. $a^C = 0$) we arrive at the expression for a point charge outside a conducting sphere

$$U_{int}(R) = \frac{q^B q^C}{R} + \frac{a^B (q^C)^2}{2}\left[\frac{1}{R^2} - \frac{1}{R^2 - (a^B)^2}\right]. \quad (3)$$

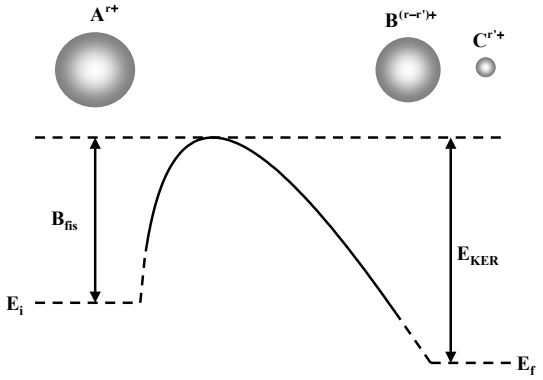

Fig. 1. Fission barrier.

When, in addition, the other sphere radius is set to zero ($a^B = 0$), equation (3) reduces to the pure Coulomb energy, $q^B q^C/R$. The total potential energy of the system, which is necessary in order to determine curve crossings between different fragmentation channels, is given by

$$U_{tot}(R) = U_{int}(R) + U_\infty, \quad (4)$$

where U_∞ is the energy required to remove q^B and q^C electrons from the spheres (B and C) at infinite center-center distance ($R = \infty$). The classical expression for the energy required to ionize a r-times charged metal sphere is given by (see e.g. [27]),

$$I_{r+1} = W + \frac{r + 1/2}{a}, \quad (5)$$

where the sum can be described as an arithmetic series,

$$\sum_{k=1}^{r} I_k = rW + r^2/2a. \quad (6)$$

Here a is the radius and W is the classical work function of the sphere. From this result, U_∞ becomes

$$U_\infty = q^B W^B + (q^B)^2/2a^B + q^C W^C + (q^C)^2/2a^C. \quad (7)$$

In Figure 1 we show a schematic of the fission barrier for the fragmentation of A ($q^A = r$) in fragments B and C with charges $q^B = r - r'$ and $q^C = r'$, respectively. The fission barrier height, B_{fis} is given by the kinetic energy release (E_{KER}) and the difference in total binding energies of the initial and final states ($E_i - E_f$), as shown in Figure 1. The fission barrier is thus

$$B_{fis} = E_{KER} - (E_i - E_f). \quad (8)$$

Here we deduce the kinetic energy release, E_{KER}, from the maximum of U_{int}(R) (fusion barrier height) as given by equation (2). The initial energy (E_i) is the sum of the binding energy of (a neutral) sphere A, E_b^A, and the energy required to remove r electrons to infinity (the sum of the ionization energies),

$$E_i = E_b^A + \sum_{k=1}^{r} I_k^A. \quad (9)$$

The final energy is

$$E_f = E_b^B + E_b^C + \sum_{k=1}^{r-r'} I_k^B + \sum_{k=1}^{r'} I_k^C, \quad (10)$$

where E_b^B and E_b^C are the binding energies of sphere B and C, respectively. With use of equation (5), the fission barrier for separating spheres with charges $r-r'$ (q^B) and r (q^C) becomes

$$B_{fis} = E_{KER} + E_a^r + r'(W^C - W^B) + (r')^2/2a^C - r'(2r - r')/2a^B, \quad (11)$$

where the activation energy for emitting a neutral fragment from a sphere of charge r (E_a^r) is given by

$$E_a^r = E_a + r(W^B - W^A) + r^2(a^A - a^B)/2a^A a^B. \quad (12)$$

Here E_a is the difference in binding energy of the final and initial states, $E_a = E_b^B + E_b^C - E_b^A$, for a neutral sphere. Note that the correction to the activation energy for a charged in relation to a neutral sphere is small, i.e. $E_a^r \approx E_a$ for the emission of a small fragment ($a^A \approx a^B$) as long as r is small.

Once the model sphere radii, a^B and a^C, have been determined, the present simple model yields the kinetic energy release and the curve crossing distances for Auto-Charge-Transfer (cf. Eq. (2)). With the additional information on the sphere work function and the activation energies for evaporation from a neutral sphere it is also possible to deduce fission barriers (cf. Eqs. (11, 12)).

3 Results and discussion

In order to determine the fragment radii and work functions we use the expression for the ionization energies (Eq. (5)) in two different approaches: (i) the radius of the C_{60} ($a^A = 7.2a_0$) is given by a fit to the sequence of experimental ionization energies [27] with the radii of the heavy and the light fragments derived from this value assuming a constant volume density. This yield $a^B = 7.2(1 - 2m/60)^{1/3}a_0$ and $a^C = 7.2(2m/60)^{1/3}a_0$, respectively. The work function is in this case assumed to be size independent ($W = 5.72$ eV). (ii) For the large fragments we use the values calculated by Leach [29], where the work functions and radii for C_{60} and C_{70} are obtained from a linear fit to the first and second experimental ionization energies. A linear interpolation and extrapolation through these values was then used to deduce the work functions and radii for C_{56} and C_{58}. Thus the work functions are size-dependent in this case. The small fragments radii and work functions in approach (ii) are derived by a linear fit to theoretical values [30] for the first and second ionization energies of C_2 and C_4. The model radii, work functions, first and second ionization energies in approach (i) and (ii) are displayed in the upper and lower part of Table 1, respectively. In [15] we deduced kinetic energy releases and fission barriers for C_2^+ emission using a slightly different approach than the two presented here. There [15] the radius of the large fragment ($a^B = 7.1a_0$) is calculated using constant *surface* density with the radius of the small ($a^C = 2.4a_0$) calculated from the experimental first ionization potential ($I_1(C_2)$) and a constant work function ($W = 5.72$ eV). This gives almost identical kinetic energy releases as the ones ((i) and (ii)) presented here.

Table 1. Model work functions (W), radii (a), first (I_1) and second ionization potentials (I_2) for different fragment products. The upper- (i) and lower-part (ii) displays the results for the approaches (i) and (ii) described in the text.

(i)	W (eV)	a (a_0)	I_1 (eV)	I_2 (eV)
C_2	5.72	2.32	11.58	23.31
C_4	5.72	2.92	10.38	19.69
C_{56}	5.72	7.04	7.65	11.52
C_{58}	5.72	7.11	7.63	11.46
(ii)	W (eV)	a (a_0)	I_1 (eV)	I_2 (eV)
C_2	6.34	2.44	11.92	23.07
C_4	7.82	3.96	11.26	18.13
C_{56}	5.80	7.27	7.67	11.41
C_{58}	5.76	7.23	7.64	11.40

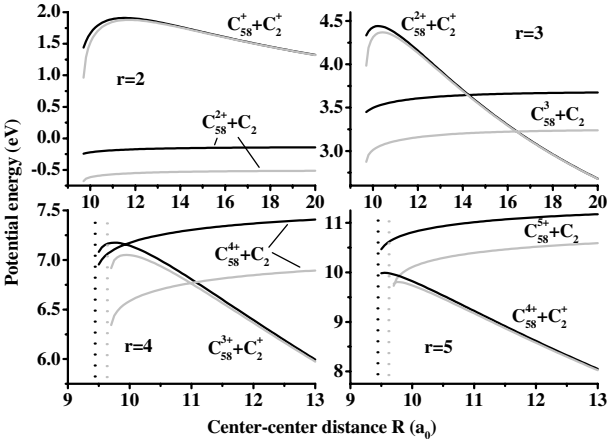

Fig. 2. Potential energy curves for neutral and singly charged C_2-emission from C_{60}^{r+} ($r = 2$–5). Black and grey full curves correspond to approach (i) and (ii), respectively. The black (i) and grey (ii) dotted lines in the two lower graphs indicates where the sphere surfaces are in contact.

The Auto-Charge-Transfer (ACT) mechanism may in principle play an important role in the determination of the kinetic energy releases. According to the present model the ACT process is only possible if the crossing of neutral and singly charged potential curves lie inside the critical distance for electron transfer, yielding a kinetic energy release which is lower than the fusion barrier height. In Figure 2 we show the relations between calculated total potential energy curves (Eq. (4)) for the C_{58}^{r+}+C_2 and $C_{58}^{(r-1)+}$+C_2^+ channels ($r = 2$–5), where the latter curves have been set to zero at $R = \infty$. The black and the

grey curves are calculated using assumptions (i) and (ii), respectively. The potential energy curves differ slightly, mainly due to the difference in ionization potentials (cf. Tab. 1). However, the conclusions are the same for both cases. In the upper left of Figure 2 ($r = 2$), there are no curve crossings and neutral emission is energetically more favourable, while the potential curves cross when $R = 14.3a_0$ (i) and $R = 16.4a_0$ (ii) for $r = 3$ (upper right). These crossings are outside the critical distance for electron transfer at $R_c = 12.5a_0$ (both approaches), suggesting that the ACT process is inactive for $r = 3$. The situation is different for the fragmentation of C_{60}^{4+} where the two channels cross around $R = 10a_0$ (i) and $R = 11a_0$ (ii), which are inside the critical distances for electron transfer at $R_c = 13.0a_0$ (i) and $R = 12.9a_0$ (ii). This means that the electron may classically move from the light to the heavy fragment at the crossing and the ACT process is thus, from these considerations, expected to be active for $r = 4$. The expected kinetic energy release would, however, be about the same as for a direct C_2^+ emission process since the potential energy at the crossing is only slightly lower than the maximum of the fission potential energy curve (which defines E_{KER} for the direct process). The lower right figure shows that the fission potential energy curves lie below the one for evaporation for all R and thus there are no crossings and direct C_2^+-emission becomes dominant for $r \geq 5$.

3.1 Kinetic energy releases

In Figure 3, we show model- and experimental [15,26,31] kinetic energy releases for the $C_{60}^{r+} \rightarrow C_{58}^{(r-1)+} + C_2^+$ (upper) and $C_{60}^{r+} \rightarrow C_{56}^{(r-1)+} + C_4^+$ (lower) fragmentation processes as functions of the initial charge r. For the emission of a C_4^+-unit, our calculations show that there are no curve crossings regardless of r and the approach ((i) or (ii)) used. Thus all model values displayed in Figure 3 are given by the maxima of the fission potential energy curves. The experimental measurements give similar kinetic energy releases for C_2^+- and C_4^+-emission [15,26,31], which is also the case for the model approach (i). In approach (ii), on the other hand, the difference is more pronounced due to the larger radius of C_4^+, yielding lower kinetic energy releases. It is interesting to note that all model values, given without the ACT concept, are in good agreement with the experimental results presented by Senn et al. [31]. The trend, however, is that the model values for both approaches are higher than the experimental values, which may be due to the fact that electronic and vibrational excitations are not taken into account in the present model. An increase in the excitation energy after the decay would lead to lower kinetic energy release values [15].

The radius of a conducting sphere (a) is related to its polarizability (α) through $a = \alpha^{1/3}$. The ratios $a(C_{2n})/a(C_{60})$ obtained from calculated polarizability values [32,33] are 0.37 ($n = 1$) and 0.45 ($n = 2$) to be compared with 0.32 ($n = 1$) and 0.41 ($n = 2$) for approach (i) and 0.34 ($n = 1$) and 0.55 ($n = 2$) for (ii).

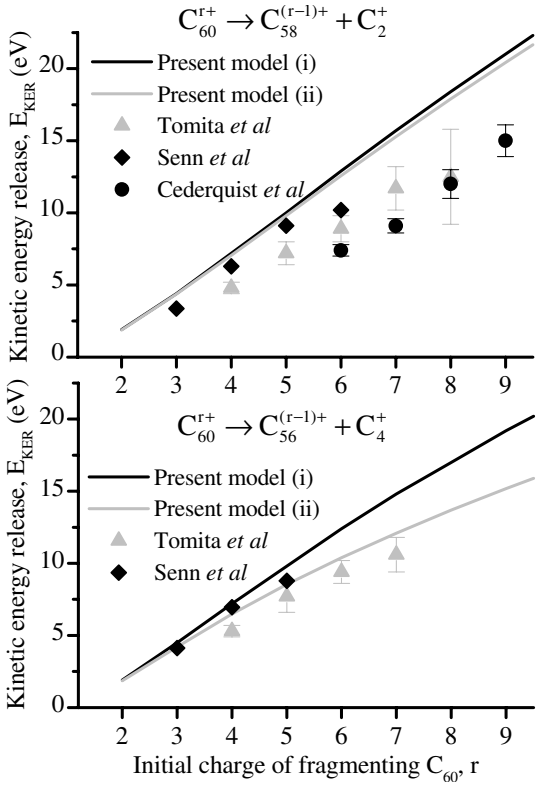

Fig. 3. Experimental [15,26,31] and model kinetic energy releases (E_{KER}) as functions of the initial charge of C_{60}, r. The upper part displays C_2^+-emission, while C_4^+-emission is shown in the lower. Black and grey curves correspond to model calculations assuming charge independent (approach (i)) and charge dependent (approach (ii)) work functions, respectively.

This comparison indicates that we perhaps overestimate the radius of C_4 in approach (ii). A common assumption in approaches (i), and (ii) is that the radii of the spheres are charge independent, which is customary in model estimates of ionization potentials for metal clusters. This also appears reasonable from the point of view of Dirac-Fock-Slater calculations [17] which predicts the *cage* radius of C_{60}^{r+} only to be slightly larger for $r = 7$ than for $r = 0$.

3.2 Fission barriers

The model fission barriers (Eq. (11)) for the processes, $C_{60}^{r+} \rightarrow C_{60-2m}^{(r-1)+} + C_{2m}^+$ ($2m = 2-4$), as functions of the initial charge state r are displayed in Figure 4, where the upper part corresponds to approach (i) and the lower to approach (ii). The activation energies are assumed to be charge independent ($E_a^r = E_a$) and charge dependent in the left and right columns, respectively. Activation energies for neutral C_2- and C_4-emission from neutral C_{60}, $E_a(C_2) = 9$ eV and $E_a(C_4) = 11.8$ eV, are extracted from calculated binding energies of carbon clusters ranging from C_3 to C_{60} [34] and C_2 [35]. Recent measurements [36,37] and calculations [16,38] of $E_a(C_2)$, give a value between 10 eV and 12.5 eV. Thus the activation energies used here are slightly lower. Below we will, however,

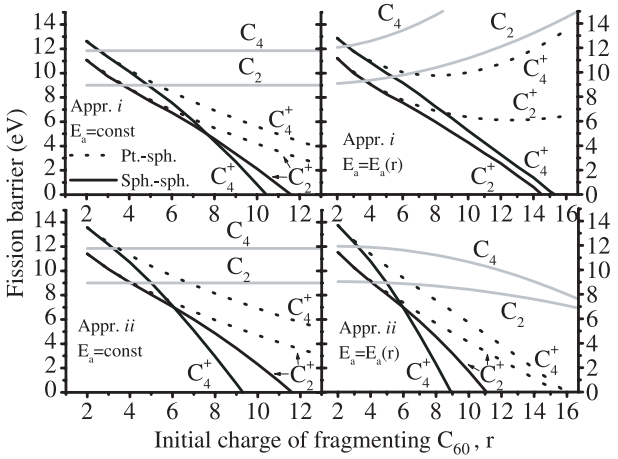

Fig. 4. Model fission barriers in the asymmetric fission processes, $C_{60}^{r+} \rightarrow C_{60-2m}^{r+} + C_{2m}^{+}$ ($2m = 2-4$), as functions of the initial charge r. The activation energies are assumed to be charge independent and charge dependent, in the left and right column, respectively. The present sphere-sphere (sph.-sph.) model results are obtained using a size independent (upper) and a size dependent (lower) work function. We also show results for a point charge and a sphere (Pt.-sph).

compare different fragmentation channels with each other and for this purpose it is only necessary to determine the difference between C_2 and C_4 activation energy for $r = 0$. In addition, a common shift of the activation energies will only have a minor effect on the stability limit predictions (the charge state when $B_{fis} = 0$), since the slopes of the fission barrier curves are rather steep. The curves in the left column of Figure 4 indicates that C_2-evaporation is dominant for $r < 4$ ((i) and (ii)) since the activation energy ($E_a(C_2)$) is lower than the fission barriers. For $r \geq 8$ (i) and $r \geq 6$ (ii), C_4^+-emission has the lowest barrier height suggesting that this is the most probable process for large r. Shown in Figure 4 as dashed curves are, in addition, calculated fission barriers obtained by considering the maximum of the interaction energies between $C_{60-2m}^{(r-1)+}$ (considered to be charged conducting spheres) and point charges.

When the charge dependent term is added to the activation energies, the fission barriers are somewhat different, as displayed in the right column of Figure 4. The charge dependence is weak for the emission of small fragments from a moderately charged parent ion. Thus all graphs in Figure 4 show the same behaviour for $r < 4$, while there are considerable differences for larger r. According to the upper graph in the right column of Figure 4, C_2^+-emission is the dominant channel for all $r \geq 4$, which is due to the larger activation energy for C_4 emission. The activation energy is in this case increasing with increasing charge state r, due to the fact that the radii of C_{56} and C_{58} are smaller than the C_{60} radius (cf. upper part of Tab. 1). In the lower right of Figure 4, on the other hand, the activation energy is decreasing with increasing charge state r. This type of behaviour is in accordance with calculations for $E_a^r(C_2)$ performed by Díaz-Tendero et al. [16], yielding 12.5 eV, 11.8 eV and 11.3 eV for $r = 0-2$. However, the difference between the sphere-sphere fission barriers in the lower part of Figure 4 are small since the r-dependence is weak for the charge states displayed. It is further interesting to note that the point-sphere model suggests C_{60}^{r+} stability limit in the range $r = 15$ to $r = \infty$ for the four graphs in Figure 4, while the present sphere-sphere model gives maximum values between $r = 9$ and $r = 14$. Thus it is clearly necessary to consider the finite size and thus the polarizabilities of the smaller fission products. The highest charge state observed for an intact C_{60}^{r+} is $r = 12$ [23], while theoretical models predict $r = 10$ [39], $r = 13$ [17], and $r = 16$ [40] for a C_{60}^{r+}-ion in its ground state. The present calculations are in qualitative agreement with these results.

Measurements of branching ratios [19,20,25,41] show that the competition between the different channels are in favor of neutral emission when $r < 4$, while the emission of one or several small charged fragments (asymmetric fission) become more dominant for $r > 4$. For large r the C_{60}^{r+} ions predominantly decay through multifragmentation (total destruction of the C_{60}-cage). Asymmetric fission processes are however observed for r up to 9 [20,21]. This indicates that C_{60}^{r+} is produced at low internal energy and the fission process for large r can be described as the emission of one charged fragment or the successive emission of several charged fragments. The branching ratios for C_4^+-emission were shown to be decreasing with increasing charge state [14], indicating that the fission barrier height decrease slower for C_4^+- compared to the C_2^+-channel. This was qualitative understood [14] using a statistical model based on Rice, Ramsperger and Kassel theory [42,43], where the channel with the lowest fission barrier will give the largest branching ratio. Note that the barrier heights calculated in [14] are deduced in a similar manner as described in the present work.

These results show that the present model calculations agree with the observed competition between evaporation and fission, while it does not reproduce the competition between C_2^+- and C_4^+-emission. Note that the discrepancy between the present model results compared to the calculations performed in [14] shows that the choice of activation and ionization energies have large influences on the conclusions about the competition between the different fission channels. Thus more precise calculations of these parameters are needed to give a more detailed description of the fragmentation process.

4 Conclusions

We have calculated kinetic energy releases and fission barriers in $C_{60}^{r+} \rightarrow C_{60}^{(r-1)+} + C_{2m}^{+}$ ($2m = 2,\ 4$) fragmentation processes, using a simple electrostatic model where the parent ion and fragment products are treated as conducting spheres. With this assumption it is possible to take the polarization of both fragments into account. Two different approaches to determine the radii of the spheres, both yield kinetic energy releases in qualitative agreement with

measurements [15,26,31]. The fission barrier predictions, however, differ significantly depending on the methods to deduce the model fragment radii and the charge-state dependence of the activation energy for neutral emission. Thus the model give estimates of the C_{60} stability limits in the range $r = 9-14$. When the polarization of the smaller fragments are neglected (modelled as point charges), the stability limits are found to be unrealistically high. This stresses the importance of considering also the polarizabilities of the smaller fragments. The autocharge transfer (ACT) process is most likely inactive in asymmetric fission except possibly for C_2^+-emission from C_{60}^{4+}, which is the only C_{60} charge state for which the potential curves for fission and evaporation cross at distances where over-the barrier electron transfer is classically allowed. As a consequence, the competition between evaporation and fission are determined by the activation energies and the fission barrier heights. Experimental kinetic energy releases and the competition between fission and evaporation are well reproduced by the present model, while the prediction of the stability limit of C_{60}^{r+} and the competition between different fission pathways are more uncertain. This emphasizes the importance of high level calculations of the activation- and ionization energies and their charge dependence for high charge states r, as performed by Díaz-Tendero et al. [16] for $r = 0-2$, in order to describe the C_{60}^{r+} fragmentation more accurately.

This work was supported by the Swedish Research Council under Contract Nos. F650-19981278 and F5102-993/2001.

References

1. I. Last, Y. Levy, J. Jortner, PNAS **99**, 9107 (2002)
2. Lord Rayleigh, Philos. Mag. **14**, 184 (1882)
3. N. Bohr, J.A. Wheeler, Phys. Rev. **56**, 426 (1939)
4. L. Meitner, O.R. Frisch, Nature **143**, 239 (1939)
5. K. Sattler, J. Muhlbach, O. Echt, P. Pfau, E. Recknagel, Phys. Rev. Lett. **47**, 160 (1981)
6. C. Bréchignac, P. Cahuzac, F. Carliez, M. de Frutos, Phys. Rev. Lett. **64**, 2893 (1990)
7. W.A. Saunders, Phys. Rev. A **46**, 7028 (1992)
8. F. Chandezon, S. Tomita, D. Cormier, P. Grübling, C. Guet, H. Lebius, A. Pesnelle, B.A. Huber, Phys. Rev. Lett. **87**, 153402 (2001)
9. V.M. Strutinsky, Nucl. Phys. A **95** (1967)
10. C. Yannouleas, U. Landmann, Phys. Rev. B **51**, 1902 (1995)
11. R.N. Barnett, U. Landmann, G. Rajagopal, Phys. Rev. Lett. **67**, 3058 (1991)
12. C. Bréchignac, P. Cahuzac, F. Carliez, M. de Frutos, R.N. Barnett, U. Landmann, Phys. Rev. Lett. **72**, 1636 (1994)
13. W. Ekardt, W.D. Schöne, J.M. Pacheo, in *Metal Clusters*, edited by W. Ekardt (Wiley, New York, 1999)
14. S. Martin, L. Chen, R. Brédy, J. Bernard, M.C. Buchet-Poulizac, A. Allouche, J. Désesquelles, Phys. Rev. A **66**, 063201 (2002)
15. H. Cederquist, J. Jensen, H.T. Schmidt, H. Zettergren, S. Tomita, B.A. Huber, B. Manil, Phys. Rev. A **67**, 062719 (2003)
16. S. Díaz-Tendero, M. Alcamí, F. Martín, J. Chem. Phys. **119**, 5545 (2003)
17. T. Bastug, P. Kurpick, J. Meyer, W.D. Sepp, B. Fricke, A. Rosen, Phys. Rev. B **55**, 5015 (1997)
18. C. Yannouleas, U. Landmann, Chem. Phys. Lett. **217**, 175 (1994)
19. S. Martin, L. Chen, A. Denis, J. Désesquelles, Phys. Rev. A **57**, 4518 (1998)
20. S. Martin, L. Chen, J. Bernard, R. Brédy, J. Désesquelles, Phys. Rev. A **62**, 022702 (2000)
21. J. Jensen, H. Zettergren, H.T. Schmidt, H. Cederquist, S. Tomita, S.B. Nielsen, J. Rangama, P. Hvelplund, B. Manil, B.A. Huber, Phys. Rev. A (submitted)
22. A. Brenac, F. Chandezon, H. Lebius, A. Pesnelle, S. Tomita, B.A. Huber, Phys. Scr. T **80**, 195 (1999)
23. V.R. Bhardwaj, P.B. Corkum, D.M. Rayner, Phys. Rev. Lett. **91**, 203004 (2003)
24. P. Scheier, B. Dünser, T.D. Märk, Phys. Rev. Lett. **74**, 3368 (1995)
25. P. Scheier, B. Dünser, T.D. Märk, J. Chem. Phys. **99**, 15428 (1995)
26. S. Tomita, H. Lebius, A. Brenac, F. Chandezon, B.A. Huber, Phys. Rev. A **67**, 063204 (2003)
27. H. Zettergren, H.T. Schmidt, H. Cederquist, J. Jensen, S. Tomita, P. Hvelplund, H. Lebius, B.A. Huber, Phys. Rev. A **66**, 032710 (2002)
28. U. Näher, S. Bjørnholm, S. Frauendorf, F. Garcias, C. Guet, Phys. Rep. **285**, 245 (1997)
29. S. Leach, Can. J. Phys. **79**, 501 (2001)
30. S. Díaz-Tendero, F. Martín, M. Alcamí, J. Phys. Chem. A **106**, 10782 (2002)
31. G. Senn, T.D. Märk, P. Scheier, J. Chem. Phys. **108**, 990 (1998)
32. K. Bonin, V. Kresin, *Electric dipole Polarizabilities of Atoms, Molecules, and Clusters* (World Scientific, Singapore, 1997)
33. A. Abdurahman, A. Shukla, G. Seifert, Phys. Rev. B **66**, 155423 (2002)
34. S. Hobday, R. Smith, J. Chem. Soc. Faraday. Trans. **93**, 3919 (1997)
35. C. Zhang, X. Xu, H. Wu, Q. Zhang, Chem. Phys. Lett. **364** 213 (2002)
36. S. Tomita, J.U. Andersen, C. Gottrup, P. Hvelplund, U.V. Pedersen, Phys. Rev. Lett. **87**, 073401 (2001)
37. S. Matt, O. Echt, P. Scheier, T.D. Märk, Chem. Phys. Lett. **348**, 194 (2001)
38. A.D. Boese, G.E. Scuseria, Chem. Phys. Lett. **294**, 233 (1998)
39. J. Cioslowski, S. Patchkovskiia, W. Thiel, Chem. Phys. Lett. A **248**, 116 (1996)
40. G. Seifert, R. Gutierrez, R. Schmidt, Phys. Lett. A **211**, 357 (1996)
41. B. Dünser, O. Echt, P. Scheier, T.D. Märk, Phys. Rev. Lett. **79**, 3861 (1997)
42. O.K. Rice, H.C. Ramsperger, J. Am. Chem. Soc. **49**, 1617 (1927)
43. L.S. Kassel, J. Phys. Chem. **32**, 225 (1928)